Dusty Hypersonic Flows

RONALD F. PROBSTEIN* AND FRANCO FASSIO†
Massachusetts Institute of Technology, Cambridge, Mass.

A study of the motions of solid particles in a dusty gas in the inviscid hypersonic shock layers of slender wedges and cones and the stagnation regions of cylinders and spheres is carried out. Particles of uniform size and with a size distribution are considered. Analytic drag laws for the particles are used for the cases of low, intermediate, and high particle Reynolds numbers. For a uniform particle size cloud the collection efficiency is shown to be expressible in terms of a single parameter embodying the particle characteristics, shock strength, and wedge or cone angle. In the case of the stagnation region solutions there is a corresponding similarity law but it is shown not to depend on the explicit form of the drag law or whether the flow is plane or axisymmetric. It is shown that when the appropriate similarity parameter is around one the collection efficiency rises rapidly from zero to one, with the rise almost discontinuous in the stagnation region cases. With a particle size distribution there is found to be very little deviation from the uniform size results at high Reynolds number and only small departures for other Reynolds number ranges.

Nomenclature

a_i = constants in analytic drag law, Eq. (2.3)
C_D = particle drag coefficient, Eq. (2.2)
E = collection efficiency
$\bar{E}$ = mean collection efficiency with size distribution, Eq. (8.2)
$f_N(r)$ = particle size distribution function, Eq. (8.1a)
K_i = particle relaxation parameters, Eq. (3.6)
L = reference length; base half-width for wedge or cone, body radius for cylinder or sphere
M = Mach number
n_i = exponents in analytic drag law, Eq. (2.3)
q = q'/u_∞
q' = relative speed between gas and particle, Eq. (3.3)
r = radius of spherical particle
r_0 = particle radius for which size distribution is maximum
δr = step size
$(\Delta r/r_0)^2$ = mean square deviation
R_b = body radius, cylinder or sphere
R_i = parameters in cone flow, Eq. (5.8)
Re = particle Reynolds number, $q'2r/\nu$
Re_L = body Reynolds number, $u_\infty L/\nu$
t = $t'u_\infty/L$
t' = time
u_∞ = freestream velocity
$\mathbf{u}$ = $\mathbf{u}'/u_\infty$
$\mathbf{u}'$ = fluid velocity
u,v = reduced fluid velocity components in x and y directions, respectively, u'/u_∞, v'/u_∞
$\mathbf{U}$ = $\mathbf{U}'/u_\infty$
$\mathbf{U}'$ = particle velocity
U,V = reduced particle velocity components in x and y directions, respectively, U'/u_∞, V'/u_∞
x,y = reduced coordinates along and normal to body surface, x'/L, y'/L
x_s,y_s = reduced shock coordinates
X_s = reduced shock coordinate for which particle passing through this point strikes rear edge of body or "end" of stagnation region
β_i = particle similitude parameters, Eqs. (6.1–6.3, and 7.18)
Δ'_m = shock stand-off distance; m = 1 cylinder, m = 2 sphere
Δ_m = Δ'_m/R_b
ϵ = density ratio across shock wave, ρ_∞/ρ
η_i = transformed normal coordinate, cone flow
θ_b = θ_c or θ_w
θ_c = cone half-angle
θ_s = shock half-angle
θ_w = wedge half-angle
ϑ = polar angle, Fig. 7
μ = viscosity behind shock
ν = kinematic viscosity, μ/ρ
ξ = x/x_s
ρ = density behind shock
ρ_p = particle density

Subscripts

i = 1 low, = 2 intermediate, = 3 high Reynolds number range
max = "end" of stagnation region
0 = velocity component ahead of shock
∞ = freestream conditions

Superscripts

$'$ = dimensional quantities
m = 1 two-dimensional case, = 2 axisymmetric case

I. Introduction

FOR vehicles flying in the atmosphere it is important to know, when they enter a dust or rain cloud, the particle trajectories relative to the surface. A quantity of particular interest is the "collection efficiency," E, defined as the ratio of the number of particles which strike the body to the number of particles which could strike it if their trajectories were straight and unaltered by the vehicle flowfield. A knowledge of the value of E for subsonic aircraft flying through rain clouds is of interest for the determination of the rate of ice deposition on the aircraft and engine surfaces.[1] It is also of importance to know what the collection efficiency is for vehicles flying hypersonically through the atmosphere because of the high impact energy of any particles striking the surface. The interaction of small high-energy particles with the vehicle could result in spalling or ablation. The present paper is concerned with the hypersonic flow problem.

Aerosol data for the atmosphere[2] indicate that in the upper part of the atmosphere (above about 30,000 ft), the "dust"

Received March 17, 1969; revision received September 11, 1969. This work has been sponsored by the Advanced Research Projects Agency (Ballistic Missile Defense Office) and technically administered by the Fluid Dynamics Branch of the Office of Naval Research under Contract Nonr-1841(93).

* Professor, Department of Mechanical Engineering. Fellow AIAA.

† Research Assistant, Department of Mechanical Engineering; presently at Bataafse Internationale Petroleum, The Hague, Holland.

environment is associated primarily with SO_4^- and NH_4^+ ions. The particle radii are generally less than 1μ with their density on the order of 2×10^{-2} $\mu g/m^3$. Rain clouds are present up to about 30,000 ft, usually in cumulonimbus form and their maximum water content is generally on the order of 10 g/m^3. Droplet radii range typically from 2 to 30μ although larger particle sizes are found. Hail is of little importance, even though it has been observed at altitudes up to 44,000 ft, primarily because its formation is rather rare. Of course, a vehicle could fly through rain where the particle sizes are considerably larger or through a man-made dust cloud environment which might result from intense explosions near the Earth's surface.

Theoretical and experimental work[3] indicate that particle-particle interactions must be taken into account when the void fraction in a gas-solid mixture, defined as the ratio of the gas volume to the mixture volume, is less than about 0.95–0.92. For spherical particles a void fraction of 0.92 corresponds to an interparticle spacing of about two diameters. From the atmospheric data given it follows that the particle densities are low enough, even in hypersonic shock layers, that particle-particle interactions which could increase the drag coefficients may be neglected.

In the analysis which follows the dust and rain particles will be treated as solid. In the case of the rain droplets this assumes that the time for evaporation of the rain droplet is large compared with the flow time and further that droplet breakup due to passage through the shock is neglected. Both evaporation and breakup will tend to decrease the particle size so that when considering rain clouds we may expect a collection efficiency somewhat lower than that calculated on the above assumption. The particles themselves will be taken as spherical with the drag coefficients on the particles corresponding to low, intermediate and high Reynolds number continuum flow conditions. In addition, heat-transfer effects, which are small in the present problem, will be neglected. Finally, the mass rate of flow of the particles is taken to be small in comparison with the mass rate of flow of the gas so that the particles themselves do not affect the inviscid gas motion.[4,5] This condition is always satisfied for atmospheric conditions.

II. Particle Drag Coefficients

In Fig. 1 is shown the standard drag coefficient curve for a single smooth sphere in steady incompressible flow.[3] We are concerned with the low-speed drag curve since the appropriate velocity is the relative velocity between the gas and the particles, which is subsonic for the problem considered. Here, the drag coefficient C_D is based on the projected area of the particles and the Reynolds number is defined by

$$Re = q'2r/\nu \tag{2.1}$$

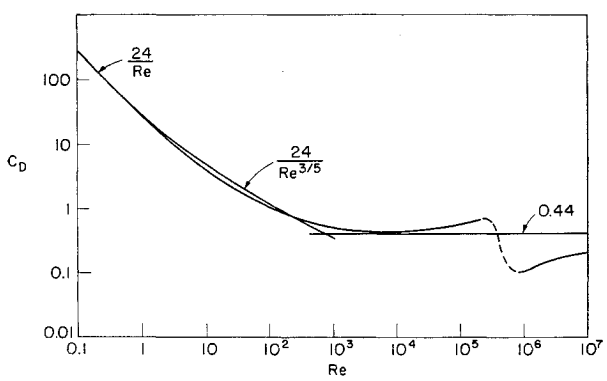

Fig. 1 Standard drag curve for a sphere.

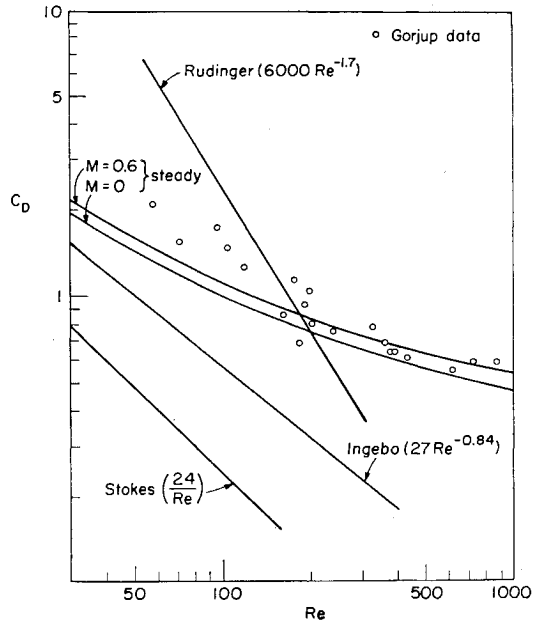

Fig. 2 Drag coefficient for a sphere.

where q' is taken to be the relative velocity, $2r$ the sphere diameter, and ν the kinematic viscosity.

For purposes of analysis it is convenient to represent the drag coefficient curves of Fig. 1 analytically in the form[6]

$$C_D = a_i Re^{-n_i} \tag{2.2}$$

Here $i = 1, 2, 3$ refers to the low, intermediate, and high Reynolds number ranges, respectively, i.e.,

$$Re < 1, \quad a_1 = 24, n_1 = 1 \tag{2.3a}$$

$$1 < Re < 10^3, a_2 = 24, n_2 = \tfrac{3}{5} \tag{2.3b}$$

$$Re > 10^3, \quad a_3 = 0.44, n_3 = 0 \tag{2.3c}$$

The values of a_2 and a_3 are empirically matched constants, the values of which can be changed without in any way altering the analysis or results which follow (though this is not quite true for n_2 and n_3). For example, a somewhat different value might represent more accurately the drag coefficient in a particular Reynolds number range of interest. Thus, in Ref. 6, a_2 is taken equal to 18.5. We have here set $a_3 = 0.44$ for consistency with the value adopted in the two phase flow literature for the so-called "Newton's law region."[3,6] Eqs. (2.2) and (2.3) are superposed on the drag curve of Fig. 1.

In the present analysis we shall assume that the drag force exerted on a particle along its trajectory corresponds to only one of the three regimes defined by Eqs. (2.3). For low values of the collection efficiency, when the particle path is long, the particle Reynolds number can decrease from very high values to values below one, so that the assumption of an unchanged drag coefficient law is not valid. In such a case the collection efficiency would be lower than that given, say, by the C_D constant or intermediate law results. However, since this behavior is likely to take place at low values of the collection efficiency the basic over-all results probably should not be greatly affected.

Some differences appear to exist in the literature concerning the appropriate drag coefficient on particles in a dusty gas, with the differences ascribed to the "unsteady" nature of the flow and electrostatic charge effects. In Fig. 2 are plotted some results for the so-called "unsteady drag coefficient" of a sphere. Ingebo[7] studied the accelerated motion of particles in subsonic flow and found the drag coefficient to be the same for both evaporating and nonevaporating par-

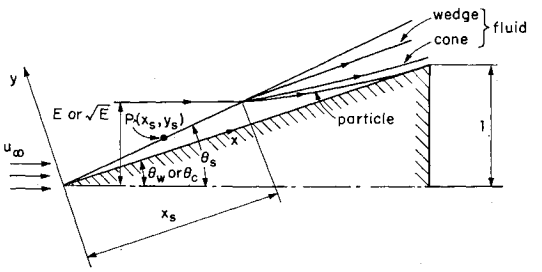

Fig. 3 Dusty flow on a wedge or cone.

ticles but found the drag to be less than in the "steady case." Rudinger[8] and Gorjup[9] studied the motion of particles accelerated by a shock wave in a shock tube and found the drag coefficient to be larger than in the steady case. Rudinger indicated that these results might be explained in terms of electrostatic charges on the particles while Gorjup explained the higher drag coefficients in terms of unsteadiness of the motion.

Recently Selberg and Nicholls[10] pointed out that the higher drag coefficients which they obtained in a set of experiments, similar to those of Rudinger and Gorjup, was due to the roughness of the surface of the particles and not to the unsteadiness of the motion, which was shown to have only a negligible effect on the drag coefficient for the conditions of the tests. It should be pointed out that the test conditions of Selberg and Nicholls were similar to those of Refs. 8 and 9. It was also shown in Ref. 10 that even for a particle Mach number less than 0.3, there was a dependence of C_D on the Mach number, with the drag coefficient increasing with increasing Mach number. It would therefore appear that the experiments of Rudinger and Gorjup can be explained in terms of the roughness of the particles and the effect of compressibility rather than any unsteadiness of the flow.

To clarify the statements, we note that roughness can provoke a local separation or the boundary layer in the region of accelerating flow past a sphere, with a consequent increase in C_D, if the dimension of the roughness is of the order of or greater than the boundary layer thickness. The HP 295 ball powder particles, used in the Selberg and Nicholls tests, which gave the highest values of C_D, compared with the less rough glass beads and sapphire balls, can have a deviation from a spherical form which can be as much as $\frac{1}{4}$ of the radius of the particle, a value much greater than any characteristic boundary layer thickness. It follows that local separation due to the roughness can take place near the stagnation point, with the result that there will be a sharp increase in the drag coefficient compared to the case where the flow remains attached.

No data are available for the experiments of Rudinger to check the effect of the particle Mach number. However, the experiments of Gorjup were run for the Mach number range $0.51 \leqslant M \leqslant 0.69$ ($50 < Re < 1000$). By using the (C_D, Re) curve for $M = 0.6$ in Ref. 11 and extrapolating it for Re less than 200, we obtain the drag coefficient curve shown in Fig. 2. This curve is seen to fairly well approximate the results of Gorjup, obtained for the experiments using smooth glass beads.

In Ingebo's experiments, which were made at flow velocities from 100 to 180 fps, the Mach number is of no importance, and the lower values of C_D may be explained in terms of the turbulence of the flow. In those tests the flow Reynolds numbers in the test pipe were in the range of 4 to 7×10^5 so that the stream was probably turbulent, particularly since the flow circuit was curved. If we consider the flow to be turbulent, then the results of Ingebo agree with those of other experimenters who used turbulent streams and got lower drag coefficients than in the laminar case, because separation over the particles is delayed with a resultant decrease in the form drag.

III. Equation of Motion for Particle

Based on the assumptions already noted the equation of motion for a single particle is written simply as a balance between the inertial force and drag on the particle. The drag coefficient expressions given by Eq. (2.2) are used, with the appropriate value of C_D depending on the Reynolds number range of interest. In the present analysis we shall restrict our considerations to the cases of plane and axisymmetric flow.

The basic equation of motion for all of the Reynolds number ranges may be written

$$\tfrac{4}{3}\pi r^3 \rho_p (d\mathbf{U}'/dt') = \tfrac{1}{2} C_D \rho \pi r^2 q' (\mathbf{u}' - \mathbf{U}') \tag{3.1}$$

with ρ_p the particle density. Here $\mathbf{U}'$ is the particle velocity

$$\mathbf{U}' = d\mathbf{x}'/dt' \tag{3.2}$$

and $\mathbf{u}'$ the gas velocity. The primes are here used to denote dimensional variables. The relative speed between the gas and the particle is given by

$$q' = [(\mathbf{u} - \mathbf{U}') \cdot (\mathbf{u}' - \mathbf{U}')]^{1/2} \tag{3.3}$$

We next write the equation of motion Eq. (3.1) for the three Reynolds number ranges considered, having first reduced it to dimensionless form by introducing the following reduced variables

$$\mathbf{U} = \mathbf{U}'/u_\infty, \ \mathbf{u} = \mathbf{u}'/u_\infty, \ q = q'/u_\infty, \ \mathbf{x} = \mathbf{x}'/L, \ t = t' u_\infty/\mathrm{L} \tag{3.4}$$

where L is a characteristic reference length and u_∞ the flow velocity at upstream infinity. Using Eq. (2.2) we obtain

$$K_i (d\mathbf{U}/dt) = q^{1-n_i} (\mathbf{u} - \mathbf{U}) \tag{3.5}$$

Here, the relaxation parameters K_i are given by

$$K_i = (2^{3+n_i}/3a_i)(\rho_p/\rho) \ (r/L)^{1+n_i} Re_L^{n_i} \tag{3.6}$$

where a_i and n_i are the analytic drag relation constants defined by Eqs. (2.3). It is apparent from Eq. (3.6) why the absolute value of a_i does not affect the form of the solution. The Reynolds number Re_L is based on the density ρ and viscosity μ behind the shock

$$Re_L = \rho L u_\infty/\mu \tag{3.7}$$

The parameters K_i measure the ability of the particle to adjust to the local gas velocity.[1,4,5] The condition $K_i \ll 1$ corresponds to the particle equilibrating rapidly to the gas velocity, $K_i \gg 1$ to the particle taking a long time to equilibrate to the gas motion, and $K_i \sim 0(1)$ to the particle being influenced by the whole history of the motion.

IV. The Wedge

In hypersonic flow the approximation that the flow is at a constant density is a useful one for many aerodynamic shapes, and in the case of flow past a wedge is exact.[12] To simplify the details of the present analysis but still bring out the essential features of the problem we shall restrict our considerations to constant density dusty hypersonic flow on slender wedges and cones, and two-dimensional or axisymmetric stagnation regions. Prior to crossing the shock wave generated by the body the particle motion is assumed unaffected by the presence of the body. Further, as noted earlier, the mass rate of flow of the particles is sufficiently small compared to that of the gas that the inviscid hypersonic solutions are unaffected by the presence of the particles. At first, we take the particles to be of uniform size, though this restriction will be dropped later and the consequences of a particle size distribution examined.

To illustrate the method of solution we first consider the flow past a slender symmetric wedge of half-angle θ_w (see

Fig. 3). The shock angle θ_s, on neglecting higher order terms [see Eq. (4.1.10) of Ref. 12] is given by

$$\theta_s \approx \theta_w/(1 - \epsilon) \tag{4.1}$$

with $\epsilon = \rho_\infty/\rho$ the density ratio across the shock.

Ahead of the shock wave, denoted by the subscript zero, the particle and fluid velocities are the same, so that

$$U_0 = u_0 = \cos\theta_w \approx 1 \tag{4.2}$$

$$V_0 = v_0 = -\sin\theta_w \approx -\theta_w \tag{4.3}$$

Here u, U, and v, V are the velocity components with respect to the x and y coordinates which are taken parallel and normal to the wedge surface, respectively, with the leading edge as origin (see Fig. 3). To the present order, behind the shock wave the fluid velocity parallel to the surface remains unchanged and equal to the freestream velocity, i.e.,

$$u = 1 \tag{4.4}$$

For the wedge, since the flow is everywhere parallel to the surface,

$$v = 0 \tag{4.5}$$

In the shock layer the difference $u - U$ is $0(\epsilon\theta_w^2)$ or smaller so that throughout the layer

$$u = U = 1 \tag{4.6}$$

Since a particle is unaffected until it passes through the shock we have from Eq. (4.4) the initial condition

$$V(x_s,y_s) = -\theta_w \text{ at } t = 0 \tag{4.7}$$

Here, x_s and y_s are reduced coordinates of a point P on the shock wave (see Fig. 3), with the characteristic length L [see Eq. (3.4)] taken to be the half-width of the base of the wedge.

As noted, of particular interest is the collection efficiency E. This quantity is determined by the trajectory of that particle which at time $t = 0$ is at the shock position X_s and which just strikes the base of the wedge at the position $x = 1/\theta_w$. From the geometry of Fig. 3 and using Eq. (4.1), the ratio of particles collected to those that would be collected if they moved in straight line trajectories is given by

$$E_i = X_s\theta_w/(1 - \epsilon) \ (i = 1,2,3) \tag{4.8}$$

The subscript i denotes the collection efficiency corresponding to the Reynolds number ranges of Eqs. (2.3.).

We next introduce the inviscid wedge solution into the equation of motion Eq. (3.5) to determine the component equations governing the particle velocities and trajectories. From Eqs. (4.5) and (4.6) the component equations of motion are

$$U = 1 \tag{4.9}$$

$$K_i(dV/dt) = (-V)^{2-n} \tag{4.10}$$

With $U = dx/dt$, Eq. (4.9) gives

$$x - x_s = t \tag{4.11}$$

for $t = 0$ at the shock. Using the initial condition Eq. (4.7) and $V = dy/dt$, Eq. (4.10) can be integrated twice with the following results:

Stokes flow ($Re < 1$)

$$V = -\theta_w e^{-t/K_1} \tag{4.12}$$

$$y_s - y = K_1\theta_w(1 - e^{-t/K_1}) \tag{4.13}$$

Intermediate law ($1 < Re < 10^3$)

$$V = -\theta_w[1 + \tfrac{2}{5}(\theta_w^{2/5}/K_2)t]^{-5/2} \tag{4.14}$$

$$y_s - y = \tfrac{5}{3}K_2\theta_w^{3/5}\{1 - [1 + \tfrac{2}{5}(\theta_w^{3/5}/K_2t]^{-3/2}\} \tag{4.15}$$

C_D constant ($Re > 10^3$)

$$V = -(K_3\theta_w)/(\theta_w t + K_3) \tag{4.16}$$

$$y_s - y = K_3 \ln[1 + (\theta_w t/K_3)] \tag{4.17}$$

The collection efficiency as defined through Eq. (4.8) is determined by eliminating t in Eqs. (4.13, 4.15, or 4.17) (depending on the case) using Eq. (4.11) after having set $x_s = X_s$ and $x = 1/\theta_w$, with X_s given by Eq. (4.8). Setting $y_s = (\theta_s - \theta_w)\,X_s$, $y = 0$ and using Eq. (4.1) the following expressions for the collection efficiency are found

$$E_1 = \frac{K_1\theta_w}{\epsilon}\left\{1 - \exp\left[-\frac{1 - (1 - \epsilon)E_1}{K_1\theta_w}\right]\right\} \qquad (Re < 1) \tag{4.18}$$

$$E_2 = \tfrac{5}{3}\frac{K_2\theta_w^{3/5}}{\epsilon}\left\{1 - \left[1 + \tfrac{2}{5}\frac{1 - (1 - \epsilon)E_2}{K_2\theta_w^{3/5}}\right]^{-3/2}\right\} \qquad (1 < Re < 10^3) \tag{4.19}$$

$$E_2 = \frac{K_2}{\epsilon}\ln\left[1 + \frac{1 - (1 - \epsilon)E_3}{K_3}\right] \qquad (Re > 10^3) \tag{4.20}$$

V. Cone

The determination of the basic equations for the case of the right circular cone parallels that for the wedge. The cone half-angle is denoted by θ_c. The relation between the shock angle and body angle is the same as for the wedge with ϵ reduced by a factor of $\frac{1}{2}$ (see Ref. 12, p. 227)

$$\theta_s = \theta_c/[1 - (\epsilon/2)] \tag{5.1}$$

Ahead of the shock wave, Eqs. (4.2) and (4.3) still apply with θ_w replaced by θ_c. Behind the shock, within the constant density approximation, the streamlines are hyperbolas with the body surface as asymptote.[12] The velocity component parallel to the surface is approximately constant with x and equal to the freestream velocity so that, as for the wedge, Eq. (4.6) holds throughout the shock layer. On the other hand, the velocity component normal to the surface varies linearly with y, i.e.,

$$v = -y/x \tag{5.2}$$

The initial condition Eq. (4.7) is also the same as for the wedge, with θ_w replaced by θ_c. The collection efficiency is readily shown to be given by (cf. Fig. 3)

$$E_i = [X_s\theta_c/(1 - \tfrac{1}{2}\epsilon)]^2 \tag{5.3}$$

Introducing the inviscid cone solution [Eqs. (4.6) and (5.2)] into the equation of motion Eq. (3.5), the component differential equations governing the particle trajectories reduce to Eq. (4.9) and the second-order equation

$$K_i(d^2y/dx^2) = \left(-\frac{y}{x} - dy/dx\right)^{2-n_i} \tag{5.4}$$

Here d/dt has been replaced by d/dx (since $U = dx/dt = 1$).

In general, Eq. (5.4) must be solved numerically. For convenience of solution the following change of variables is introduced

$$\xi = \frac{x}{x_s},\ \eta_1 = \frac{y}{K_1\theta_c},\ \eta_2 = \frac{yx_s^{3/2}}{K_2^{5/2}},\ \eta_3 = \frac{y}{K_3} \tag{5.5}$$

where x_s is treated as a parameter. Equations (5.4) then become

$$R_1(d^2\eta_1/d\xi^2) = -d\eta_1/d\xi - \eta_1/\xi \tag{5.6a}$$

$$d^2\eta_2/d\xi^2 = (-d\eta_2/d\xi - \eta_2/\xi)^{2/5} \tag{5.6b}$$

$$d^2\eta_3/d\xi^2 = (-d\eta_3/d\xi - \eta_3/\xi)^2 \tag{5.6c}$$

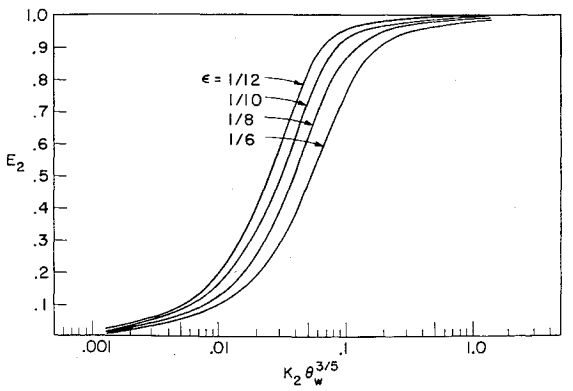

Fig. 4 Wedge collection efficiency for intermediate law.

The initial conditions obtained from Eqs. (4.7) and (5.1) are

$$\eta_i = R_i \frac{\frac{1}{2}\epsilon}{1 - \frac{1}{2}\epsilon}, \frac{d\eta_i}{d\xi} = -R_i \text{ at } \xi = 1 \tag{5.7}$$

Here

$$R_1 = \frac{x_s}{K_1} = \frac{x_s\theta_c}{K_1\theta_c} \tag{5.8a}$$

$$R_2 = \theta_c\left(\frac{x_s}{K_2}\right)^{5/2} = \left(\frac{x_s\theta_c}{K_2\theta_c^{3/5}}\right)^{5/2} \tag{5.8b}$$

$$R_3 = x_s\theta_c/K_3 \tag{5.8c}$$

Equations (5.6) may be solved numerically‡ for a fixed value of R_i and ϵ. This procedure was carried out and the integration stopped when $\eta = 0$, i.e., when the particle strikes the surface. The value of ξ so determined enables the collection efficiency to be calculated from

$$E_i = [\xi(1 - \tfrac{1}{2}\epsilon)]^{-2} \tag{5.9}$$

This relation follows from Eq. (5.3) with $x = 1/\theta_c$. For this case $x_s = X_s$ so that knowing E_i and R_i enables the determination from Eq. (5.3) and Eqs. (5.8) of the value of the parameter upon which E_i depends. In addition to ϵ, the parameter is seen to be $K_1\theta_c$, $K_2\theta_c^{3/5}$, or K_3, respectively, for $i = 1, 2,$ or 3.

VI. Similitudes and Numerical Results for Wedges and Cones

The parameters which, in general, determine the collection efficiency of both wedges and cones are the strength of the shock characterized by the density ratio ϵ, the body angle θ_w or θ_c, and the particle characteristics as specified by the parameters K_i. We note, however, in the relations for the wedge collection efficiencies, Eqs. (4.18–4.20), that θ_w enters only in Eqs. (4.18) and (4.19) and then only in the combination $K_1\theta_w$ and $K_2\theta_w^{3/5}$, while in Eq. (4.20) K_3 appears by itself. An exactly similar behavior was found for the cone, where the collection efficiency was shown to depend, in addition to ϵ, only upon $K_1\theta_c$, $K_2\theta_c^{3/5}$ and K_3, respectively.

To illustrate the behavior of E_i we have plotted in Fig. 4, using Eq. (4.19), the intermediate law wedge collection efficiency as a function of $K_2\theta_w^{3/5}$ for different values of ϵ. For all Reynolds number ranges and for both wedges and cones the curves of E_i are qualitatively similar and have the typical relaxation form shown in Fig. 4.

Although it is clear from the basic equations that there is no exact similitude for E_i which would also embody ϵ it is nevertheless apparent, e.g., from the results of Fig. 4, that the curves for E_i have a similar character for different values of ϵ. Using as a guide the asymptotic behavior of the solutions for large and small values of $K_1\theta_b$, $K_2\theta_b^{3/5}$, and K_3, where θ_b may be either θ_w or θ_c, the variation of E_i with ϵ has been found for both the wedge and cone to be empirically correlated by the following parameters:

Stokes flow $\beta_1 = K_1\theta_b/\epsilon$ (6.1)

Intermediate law $\beta_2 = K_2\theta_b^{3/5}/\epsilon^{(1+5m)/5m}$ (6.2)

C_D constant $\beta_3 = K_3/\epsilon^{(1+2m)/2m}$ (6.3)

where $m = 1$ for the wedge and $m = 2$ for the cone. Thus

$$E_i = E_i(\beta_i)$$

alone for all K_i, θ_b, ϵ and for wedge or cone flow.

In Figs. 5 and 6 are plotted for the wedge and cone, respectively, the collection efficiency as a function of β_i for the three Reynolds number ranges considered. Numerical calculations of E_i were carried out for values of ϵ in the range $\frac{1}{12} \leqslant \epsilon \leqslant \frac{1}{6}$ and the correlation of these results by use of the parameters of Eqs. (6.1–6.3) is sufficiently accurate that only a single curve is shown for each of the three different drag law ranges. It is clear from these curves that for both the wedge and cone, when the value of the relaxation parameters $\beta_i \sim 0(1)$ that $E_i \sim 0(1)$. In other words, the parameters β_i are the appropriate relaxation parameters which replace K_i for the particular cases of dusty hypersonic flow on slender wedges and cones.

One interesting fact, which is not explained, is that for both the wedge and cone the value of E_i for all three drag laws is the same for $\beta_i \approx 0.6$, though the value of E_i at this point is 50% greater for the cone than the wedge.

VII. Stagnation Region of a Sphere and Cylinder

We next consider the flow in the stagnation region of a cylinder and a sphere, with the approximation that the flow is one of constant density. The coordinate system used is shown in Fig. 7. Ahead of the shock wave, denoted by the subscript zero, the particle and fluid velocities (all referred to the freestream velocity u_∞) are the same, so that

$$U_0 = u_0 \approx 0 \tag{7.1}$$

$$V_0 = v_0 = -1 \tag{7.2}$$

where the x and y coordinates are taken along and normal to the body surface with the stagnation point as origin. Here u, v and U, V are the respective flow and particle velocities as before. The characteristic length $L \equiv R_b$, the body radius.

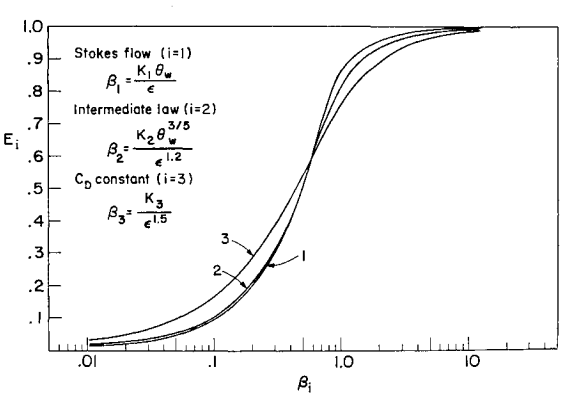

Fig. 5 Collection efficiency for wedge.

‡ Equation (5.6a) is linear and can be integrated directly while Eq. (5.6c) is reducible to an equation of first order. In both cases, however, the collection efficiency still has to be determined numerically. It was therefore found more convenient to carry out the integration of all of Eqs. (5.6) with the same numerical procedure.

Since the flow is hypersonic we may make the approximation that behind the shock wave

$$V \gg u,v,U \tag{7.3}$$

Therefore, the relative speed between the gas and particle is simply the freestream velocity or

$$q = 1 \tag{7.4}$$

In this case the component equations of motion for the particle all have the same form, independent of the drag law, i.e., Eq. (3.5) becomes

$$K_i(dU/dt) = u - U \tag{7.5}$$

$$K_i(dV/dt) = -V \tag{7.6}$$

The initial and boundary conditions are

$$U(x_s,y_s) = 0,\ V = -1,\ y = \Delta_m \text{ at } t = 0 \tag{7.7}$$

Here, Δ_m is the reduced stand-off distance of the shock wave measured in body radii (Δ'_m/R_b, see Fig. 7) with the subscript $m = 1$ for the cylinder and $m = 2$ for the sphere.

Integrating Eq. (7.6) subject to the initial condition Eq. (7.7) on V we find

$$V = -e^{-t/K_i} \tag{7.8}$$

On applying the definition $V = dy/dt$ and integrating Eq. (7.8) subject to the condition $y = \Delta_m$ at $t = 0$

$$\Delta_m - y = K_i(1 - e^{-t/K_i}) \tag{7.9}$$

The condition $y = 0$ can clearly only be satisfied for values of $K_i > \Delta_m$, i.e., within the present approximation no particles will strike the surface for $K_i \leq \Delta_m$.

The polar angle ϑ_{max} (see Fig. 7b) is defined as the angle for which the local stagnation point solution may no longer be applied (say, 15–20°) with x_{max} the corresponding length of the arc DF. The stand-off distance Δ_m is small compared with 1 and within the simple constant density theory the shock is parallel to the body surface so that the arc AB on the shock may be approximated by the arc DC on the body. In this case, if B is the point at which a particle striking the body at F enters the shock layer, and if we define $AB = CD = X_s$, the collection efficiency is simply given by

$$E_i = (X_s/x_{\max})^m \tag{7.10}$$

where again $m = 1$ for the cylinder and $m = 2$ for the sphere.

We next solve Eq. (7.5) for the cases of the cylinder and sphere by introducing the solutions for the flow velocity obtained from the constant-density theory.

1. Cylinder

From Ref. 12, on neglecting terms of order higher than ϵ and $\epsilon \ln(1/\epsilon)$, the x component of the velocity is given by

$$u = (3\epsilon)^{1/2}\, x \cosh[(y/\epsilon)f(\epsilon)] \tag{7.11a}$$

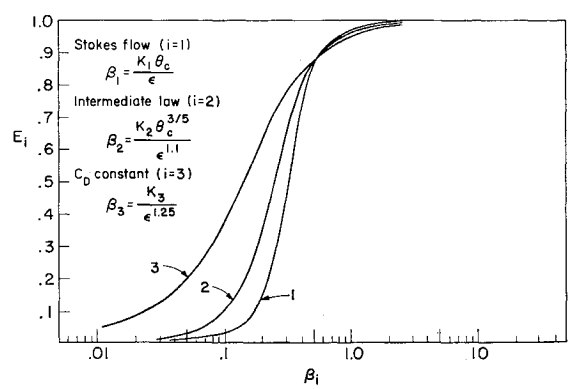

Fig. 6 Collection efficiency for cone.

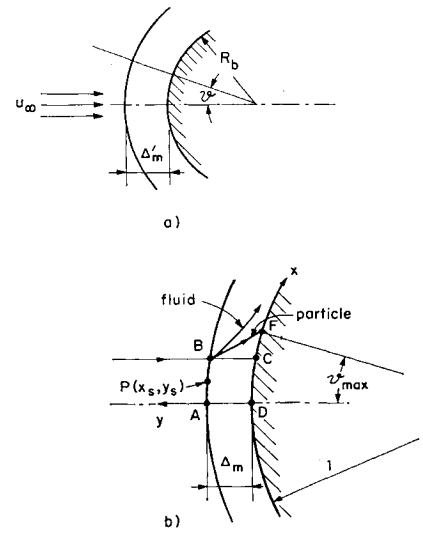

Fig. 7 Coordinates for stagnation region of a cylinder or sphere: a) dimensional, b) dimensionless.

where

$$f(\epsilon) = (1 - \tfrac{1}{2}\epsilon \ln(4/3\epsilon) - \tfrac{3}{2}\epsilon) \tag{7.11b}$$

To consistant order the stand-off distance is

$$\Delta_1 = \frac{1}{2}\epsilon \ln\frac{4}{3\epsilon} \tag{7.12}$$

Using Eqs. (7.9, 7.11, and 7.12) the x component of the equation of motion Eq. (7.5) reduces to

$$K_i\frac{d^2\xi}{dt^2} + \frac{d\xi}{dt} - (3\epsilon)^{1/2}\xi \cosh\left\{\left[\frac{1}{2}\ln\frac{4}{3\epsilon} - \frac{K_i}{\epsilon}(1 - e^{-t/K_i})\right] f(\epsilon)\right\} = 0 \tag{7.13}$$

Here, ξ has the same definition as in Eq. (5.5). Equation (7.13) is solved numerically subject to the initial conditions

$$\xi = 1 \text{ and } d\xi/dt = 0 \text{ at } t = 0 \tag{7.14}$$

The collection efficiency is obtained by stopping the integration at the time t for which $y = 0$ [see Eq. (7.9)]. The value of $\xi_{max} = x_{max}/X_s$ thus found determines from Eq. (7.10) (with $m = 1$) the collection efficiency.

2. Sphere

From Ref. 12 the corresponding solution for the sphere is given to $0(\epsilon^{3/2})$ by

$$u = (\tfrac{8}{3}\epsilon)^{1/2}(1 - \epsilon)x + (xy/\epsilon)g(\epsilon) \tag{7.15a}$$

where

$$g(\epsilon) = 1 - \tfrac{14}{3}\epsilon + 2\epsilon(\tfrac{8}{3}\epsilon)^{1/2} \tag{7.15b}$$

To consistent order the stand-off distance is

$$\Delta_2 = \epsilon[1 - (\tfrac{8}{3}\epsilon)^{1/2}] \tag{7.16}$$

In a manner similar to that for the cylinder, Eq. (7.5) reduces to

$$K_i\frac{d^2\xi}{dt^2} + \frac{d\xi}{dt} - \xi\left[\frac{11}{3}\epsilon\left(\frac{8}{3}\epsilon\right)^{1/2} + \left\{1 - \frac{K_i}{\epsilon}(1 - e^{-t/K_i})\right\}g(\epsilon)\right] = 0 \tag{7.17}$$

The initial conditions Eq. (7.14) apply in this case as well and the integration is carried out in the same manner as for the cylinder. Equation (7.10) with $m = 2$ defines the collection efficiency.

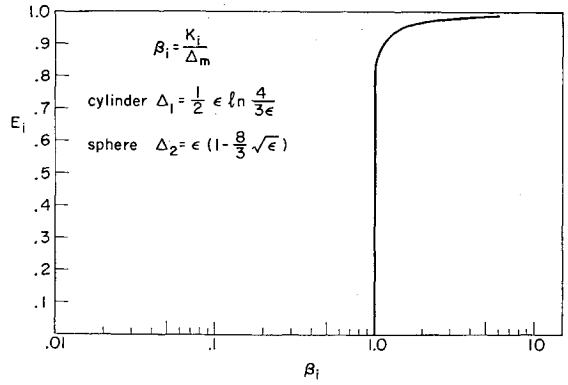

Fig. 8 Collection efficiency for stagnation region of cylinder or sphere.

Numerical integrations of Eqs. (7.13) and (7.17) have been carried out for $\frac{1}{12} \leqslant \epsilon \leqslant \frac{1}{6}$. For $K_i \to 0$ care must be taken in the integration since the problem is a singular one. However, as already pointed out, there is no solution for $K_i \leqslant \Delta_m$, though Δ_m is a small quantity of $0(\epsilon)$ or $0(\epsilon \ln 1/\epsilon)$. We note from Eqs. (7.8) and (7.9) that for $K_i \to \Delta_m$, with $y = 0$, that $V \to 0$. In this case Eq. (7.3) is no longer satisfied. In any exact solution, therefore, we may expect finite but asymptotically small values of E_i even for K_i less than Δ_m.

In Fig. 8 the collection efficiency has been plotted for both the sphere and cylinder as a function of the relaxation parameter

$$\beta_i = K_i/\Delta_m \tag{7.18}$$

This parameter was found to very good approximation to correlate in a single curve all of the numerical results for the range of ϵ considered. We note from this curve, for values of the relaxation parameters K_i slightly greater than Δ_m, that there is a very sharp rise in the collection efficiency, with the collection efficiency essentially becoming equal to unity for all $K_i > \Delta_m$. This contrasts with the much smoother "transition" for the cases of the wedge and cone. However, the fact that again $E_i \sim 0(1)$ for $\beta_i \sim 0(1)$, as with the wedge and cone, indicates that the parameters β_i as defined are the appropriate relaxation parameters for stagnation region dusty hypersonic flows.

It may be expected that a more realistic flowfield solution, including the effects of nonconstant density, etc., would not strongly affect the result of Fig. 8, provided the stand-off distance used is the one corresponding to the more accurate flow field solution.

VIII. Distribution of Particle Size

In this section we treat the problem of determining how the collection efficiency is altered if the cloud consists of a distribution of particles of different sizes. We consider the particular particle size number distribution characterized by the normal distribution function (Ref. 3, pp. 5 and *ff.*)

$$f_N(r) = A_N \exp\left[-\frac{(r/r_0 - 1)^2}{2(\Delta r/r_0)^2}\right] \qquad \left(\int_0^\infty f_N(r)dr = 1\right) \tag{8.1a}$$

where

$$A_N{}^{-1} = r_0\left(\frac{\pi}{2}\right)^{1/2}\left(\frac{\Delta r}{r_0}\right)\left[1 + \operatorname{erf}\left(\frac{1}{2^{1/2}\Delta r/r_0}\right)\right] \tag{8.1b}$$

Here $(\Delta r/r_0)^2$ is the mean square deviation referred to the particle radius r_0 for which the distribution function has a maximum. Data presented in Ref. 2 show that cloud droplet and natural aerosol distributions are well represented by Eq. (8.1a) and that $\Delta r/r_0$ never exceeds 0.3–0.5.

The mean collection efficiency in the case of a distribution of sizes is defined by

$$\bar{E}_i = \int_0^\infty E_i f_N(r)\, dr \tag{8.2}$$

and in presenting our results we have plotted this quantity as a function of the similitude parameters β_i defined at the point r_0. The values of E_i have been taken from the solutions given previously for the case of uniform particle sizes. In so doing we have implicitly assumed that all of the particles which given an appreciable contribution to the integral Eq. (8.2) obey the same drag law. This is justified by the fact that the values of $\Delta r/r_0$ are relatively small thereby giving rise to relatively steep distribution functions.

In carrying out the numerical calculations the integral Eq. (8.2) has been replaced by the finite sum

$$\bar{E}_i = \sum_{r=a}^{b} E_i(r) r_0 f_N(r)\, \frac{\delta r}{r_0} \tag{8.3}$$

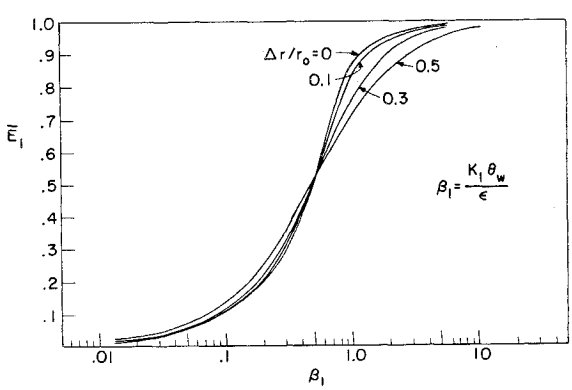

Fig. 9 Wedge collection efficiency for a particle size distribution (Stokes flow).

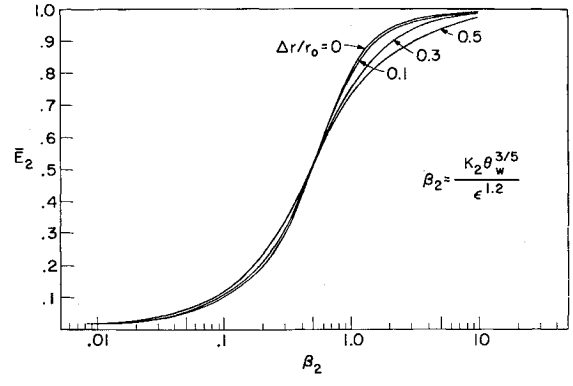

Fig. 10 Wedge collection efficiency for a particle size distribution (intermediate law).

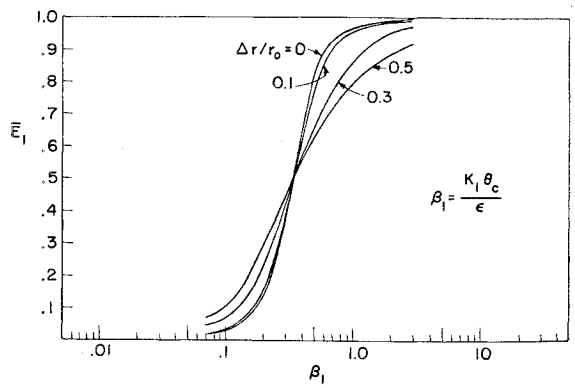

Fig. 11 Cone collection efficiency for a particle size distribution (Stokes flow).

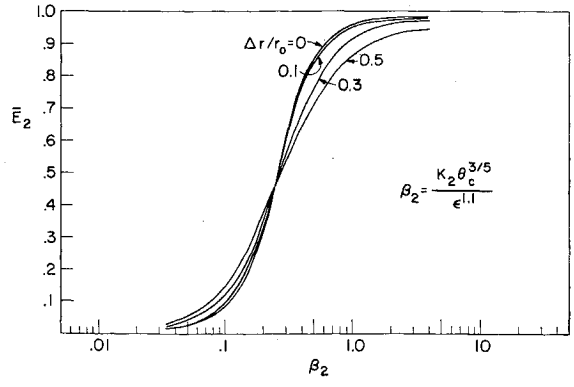

Fig. 12 Cone collection efficiency for a particle size distribution (intermediate law).

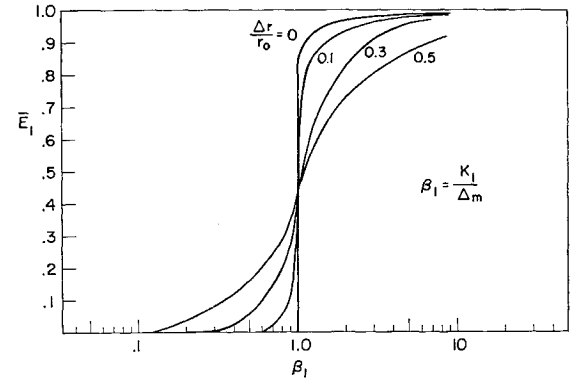

Fig. 13 Cylinder or sphere stagnation region collection efficiency for a particle size distribution (Stokes flow).

with $\delta r/r_0$ an appropriate step size. The limits of the sum represent the points for which the contribution to $\bar{E}_i$ becomes negligible. In carrying out the calculations in the interval r to $r + \delta r$, for a given r_0, $r_0 f_{r_0} f_N(r)$ was taken at the point $(r/r_0 + \frac{1}{2}\delta r/r_0)$ and E_i at the point corresponding to

$$\frac{\beta_i}{\beta_{i_0}} = \left(\frac{r}{r_0} + \frac{1}{2}\frac{\delta r}{r_0}\right)^{1+ni} \tag{8.4}$$

which follows from the fact that $\beta_i \sim K_i \sim r^{1+ni}$.

Figures 9–12 present results for the mean collection efficiency for the cases of the wedge and the cone, with Figs. 9 and 11 for a Stokes drag on the particles and Figs. 10 and 12 for the intermediate particle drag law. For the case of large particle Reynolds numbers, where the constant drag coefficient law is valid, it was found that all of the curves for $\Delta r/r_0 \leqslant 0.5$ deviate from the curves for the uniform particle size by less than 5%. For both the wedge and cone the effect of increasing $\Delta r/r_0$ is to spread out the "transition" region, a result to be expected. However, for the wedge the spread is considerably less than for the cone and in fact for $\beta_i < 0.6$ the curves all fall closely to the uniform particle size curve.

Figure 13 presents the mean collection efficiency for the stagnation region of a cylinder or sphere for the Stokes drag law. Unlike the results for the wedge and cone the curves are considerably spread out with an increasing nonuniformity in the particle size distribution. Results for the intermediate law and C_D constant are not presented though they are much less spread out than the Stokes flow case. This is due to the effect of the exponent n_i in Eq. (8.4). We note that for decreasing n_i the region of the (E_i, β_i) curves taken into account in Eq. (8.3) decreases so that the collection efficiency $\bar{E}_i$ is more dependent on the local behavior of E_i and therefore closer to the uniform size value of the collection efficiency.

It should be pointed out that for the particle distribution function used in all cases the mean collection efficiency $\bar{E}_i$ goes to zero for $\beta_i = 0$ only because $f_N \to 0$ as $r \to \infty$, so that for low but finite values of $\beta_i(r_0)$ there is still a contribution from the large values of β_i. In practice, $\bar{E}_i$ may be taken to be zero for values of β_i at most one order of magnitude less than the values which give $E_i = 0$. The reason for this is that any actual distribution function[2] will cut off at a finite particle size so that the exponential "tail" is in fact incorrect.

Finally, we note that for all cases where $\Delta r/r_0 < 0.1$, the size variation has little effect and the mean collection efficiency closely follows that for a uniform particle size.

References

[1] Taylor, G. I., "Notes on Possible Equipment and Technique for Experiments on Icing on Aircraft," R & M 2024, 1940, Aeronautical Research Committee, London.

[2] *Handbook of Geophysics and Space Environments*, edited by S. L. Valley, McGraw-Hill, New York, 1965.

[3] Soo, S. L., *Fluid Dynamics of Multiphase Systems*, Blaisdell (Ginn), Waltham, Mass., 1967.

[4] Probstein, R. F., "The Dusty Gasdynamics of Comet Heads," *Problems of Hydrodynamics and Continuum Mechanics*, edited by M. A. Lavrent'ev, Izdatel'stvo "Nauka", Moscow, 1969; English translation, SIAM, Philadelphia, 1969, pp. 568–583.

[5] Marble, F. E., "Dynamics of a Gas Containing Small Solid Particles," *Combustion and Propulsion, 5th AGARD Colloquium*, Pergamon, New York, 1963, pp. 175–215.

[6] Bird, R. B., Stewart, W. E., and Lightfoot, E. N., *Transport Phenomena*, Wiley, New York, 1960.

[7] Ingebo, R. D., "Drag Coefficients for Droplets and Solid Spheres in Clouds Accelerating in Airstreams," TN 3762, 1956, NACA.

[8] Rudinger, G., "Experiments on Shock Relaxation in Particle Suspensions in a Gas and Preliminary Determination of Particle Drag Coefficients," *Multiphase Flow Symposium*, ASME, New York, 1963.

[9] Gorjup, M., "Calibration of a Micrometeroid Impact Gauge," UTIAS TN 97, March 1967, Institute Aerospace Studies, Univ. of Toronto.

[10] Selberg, B. P. and Nicholls, J. A., "Drag Coefficient of Small Spherical Particles," *AIAA Journal*, Vol. 6, No. 3, March 1968, pp. 401–408.

[11] Goin, K. L. and Lawrence, W. R., "Subsonic Drag of Spheres at Reynolds Numbers from 200 to 10,000" *AIAA Journal*, Vol. 6, No. 5, May 1968, pp. 961–962.

[12] Hayes, W. D. and Probstein, R. F., *Hypersonic Flow Theory*, Vol. I, *Inviscid Flows*, Academic Press, New York, 1966.